



## Effect of Pore Size and Pore Wall Thickness of Mesoporous Phase in Tin Phosphate Composite on Electrochemical Cycling

Eunjin Kim,<sup>a</sup> Min Gyu Kim,<sup>b</sup> Yoojin Kim,<sup>a,b</sup> and Jaephil Cho<sup>a,\*</sup>

<sup>a</sup>Department of Applied Chemistry, Kumoh National Institute of Technology, Gumi, Korea

<sup>b</sup>Beamline Research Division, Pohang Accelerator Laboratory, Pohang University of Science and Technology, Pohang, Korea

We synthesized mesoporous/crystalline composite with a mass ratio of 1:2 (mesoporous: crystalline), and the resulting mesoporous tin phosphate has different pore size depending on the alkyl chain length ( $n = 11, 13, 15,$  and  $17$ ) of the surfactant  $\text{CH}_3(\text{CH}_2)_n\text{N}(\text{CH}_3)_3\text{Br}$ . Because the crystalline phase ( $\text{Sn}_2\text{P}_2\text{O}_7$ ) to mesoporous phase mass ratio is fixed, a decrease in the capacity retention is mainly attributed to the deterioration of the mesophase. The mesoporous phase with smaller pore size causes higher capacity retention, with  $n = 11$  showing the highest capacity retention corresponding to 82%. This decreased to 67, 63, and 59% with increasing pore size,  $n = 13, 15,$  and  $17,$  respectively.

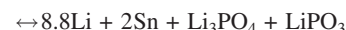
© 2005 The Electrochemical Society. [DOI: 10.1149/1.1979454] All rights reserved.

Manuscript submitted March 31, 2005; revised manuscript received May 16, 2005. Available electronically July 18, 2005.

Since the discovery of M41S silica molecular sieves in 1992,<sup>1</sup> mesoporous materials, possessing remarkably large internal surface area and narrow pore size distribution, have attracted considerable attention for their great potential application as catalysts, absorbents, and host materials. This approach to mesostructured materials has been extended to Al, Sn, and titanium phosphates and other oxides, which may lead to applications involving electron transfer or magnetic interactions.<sup>2-4</sup>

Synthesis of mesoporous materials is influenced by factors such as surfactant property, precursor/surfactant molar ratio, temperature, pressure, pH, and aging time. Cabrera et al. studied the control of pore size by varying P/Al ratio and water content in mesoporous aluminophosphate.<sup>5</sup> In addition, they reported the change in  $d$  spacing value of the mesoporous alumina upon changing TEA(triethanolamine)/water molar ratio.<sup>6</sup> Katou et al. reported that pore size, pore volume, and wall thickness of mesoporous NbTa oxide were found to be strongly affected by amounts of water and metal source in a starting ethanol solution involving nonionic surfactant P123.<sup>7</sup> Similar result was reported by Tanaka et al. and Kimura et al. by using amorphous aluminum phosphate with different alkyl group lengths. They showed that  $d$  spacing value increased in proportion to alkyl group length.<sup>8,9</sup> Serre et al. synthesized titanium fluorophosphates with hexagonal and lamellar structure by using alkyltrimethylammonium bromide [ $\text{CH}_3(\text{CH}_2)_n\text{N}(\text{CH}_3)_3\text{Br}$  with  $n = 9-17$ ] or alkylamine.<sup>10</sup> However, they only studied titanium fluorophosphates prepared using cetyltrimethylammonium bromide (CTAB), and did not observe the effect of varying the alkyl chain length on the physical properties. In addition, Mal et al. prepared alkyltrimethylammoniumbromide ( $n = 7-17$ ), but reported the  $d$  spacing value only depending on the alkyl chain length.<sup>11</sup> In summary, these studies did not further report the changes in pore size, Brunauer-Emmett-Teller (BET), and pore wall thickness with varying surfactant alkyl groups.

Contrary to conventional applications of mesoporous materials, its possible use as anode material in lithium secondary battery was reported by several groups.<sup>12-14</sup> In particular, Kim et al. reported the superior capacity retention of the mesoporous/crystalline composite consisting of tin phosphate as compared to bulk material.<sup>15</sup> They suggested that this excellent capacity retention is due to the reversibly contracting and expanding mesopores in the Li alloy/dealloy process. However, pure bulk crystalline tin phosphate ( $\text{Sn}_2\text{P}_2\text{O}_7$ ) showed quick decaying capacity even at a low C rate (20 mA/g). In general, decomposition reactions of tin phosphate were as follows<sup>16</sup>



Control of volume expansion of lithium alloying materials is a very critical issue, as smaller volume changes induce smaller capacity decay. The reason for this is believed to be pulverization of the particles due to differences in volume ( $>300\%$ ) caused by the compositional changes occurring during cycling. As the particles fragment, they become electrically isolated, which reduces the cell capacity.

In this study, different cationic surfactants  $\text{CH}_3(\text{CH}_2)_n\text{N}(\text{CH}_3)_3\text{Br}$  ( $n = 11, 13, 15,$  and  $17$ ) were used to synthesize mesoporous/crystalline tin composites with a constant mass ratio. Subsequently, we observed the effects of the different pore sizes and pore wall thicknesses of the mesoporous phase on the electrochemical cycling.

### Experimental

In a typical synthesis, the mesoporous tin phosphate- $\text{SnHPO}_4$  composite was prepared by mixing 3 g of  $\text{SnF}_2$  and 8.8 g of  $\text{H}_3\text{PO}_4$ , followed by dissolving in 10 mL of distilled-deionized water (DDW). Then, 0.0095 mol of alkyltrimethylammoniumbromide surfactant was dissolved in 10 mL of DDW, and this solution was added to the mixture solution of  $\text{SnF}_2$  and  $\text{H}_3\text{PO}_4$ . The resulting mixture was stirred at  $40^\circ\text{C}$  for 1 h, then loaded in an autoclave kept at  $90^\circ\text{C}$  for 20 h. After cooling to room temperature, the precipitate was recovered by filtration, washed with distilled water, and vacuum-dried at  $100^\circ\text{C}$  for 10 h. The as-prepared powders (mesoporous tin phosphate- $\text{SnHPO}_4$  composite) were then annealed at  $400^\circ\text{C}$  for 5 h, yielding mesoporous tin phosphate- $\text{Sn}_2\text{P}_2\text{O}_7$  composite. The electrolyte for the coin-type half cells (2016 type) was 1 M  $\text{LiPF}_6$  with ethylene carbonate/diethylene carbonate/ethyl-methyl carbonate (EC/DEC/EMC) (30: 30: 40 vol %). The coin-type half cells were cycled at a rate of 0.2 C (1 C = 700 mA/g) for the first cycle, then at a rate of 0.2 C rate for the subsequent 30 cycles between 0 and 1.5 V. The electrode was composed of 80 wt % active material, 10 wt % poly(vinylidene fluoride) binder, and 10 wt % Super P carbon black.

### Results and Discussion

Figures 1a-d exhibit small angle X-ray scattering (SAXS) patterns of the mesoporous tin phosphate prepared using dodecyl ( $n = 11$ ), myristyl ( $n = 13$ ), cetyl ( $n = 15$ ), and octadecyl ( $n = 17$ ) trimethylammoniumbromide before and after annealing at  $400^\circ\text{C}$ . As-prepared tin phosphate prepared using  $n = 11, 13,$  and  $15$  can be indexed to hexagonal cubic structure with a space group of  $Pb3/mmc$  except for  $n = 17$ .  $a$  value is identical to  $d$  spacing value

\* Electrochemical Society Active Member.

<sup>z</sup> E-mail: jpcho@kumoh.ac.kr

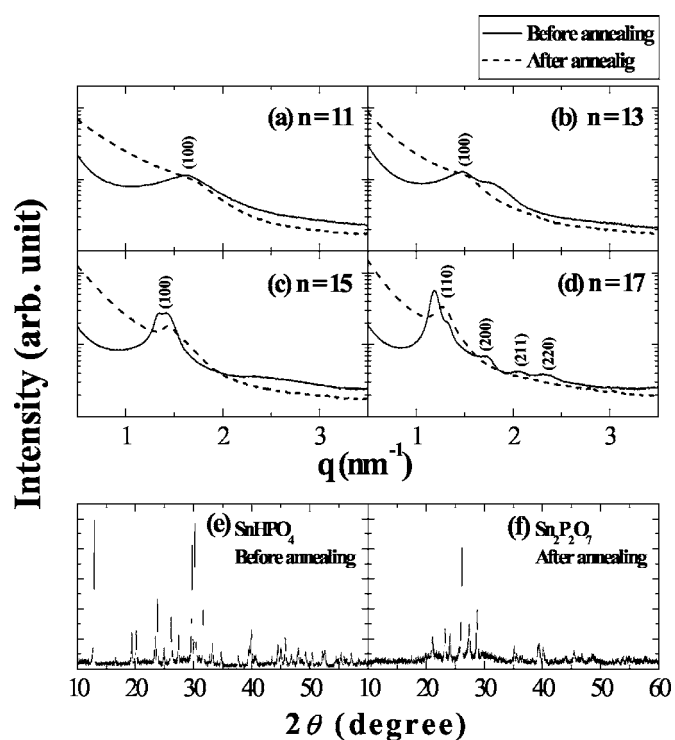


**Figure 1.** SAXS patterns of mesoporous tin phosphate/crystalline composite before and after annealing using (a)  $n = 11$ , (b)  $n = 13$ , (c)  $n = 15$ , and (d)  $n = 17$ . High angle diffraction patterns of mesoporous/crystalline composites before annealing (e), and after annealing (f) ( $q = 4\pi \sin \theta/\lambda$ ).

in the hexagonal cubic structure, showing 3.82, 4.23, and 4.55 nm for  $n = 11, 13$ , and  $15$ , respectively. SAXS pattern of  $n = 17$  before annealing shows the presence of body-centered cubic (B.C.C.) mesophase with a space group of  $Im\bar{3}m$ , and  $a$  value is estimated as 7.68 nm and  $d$  value ( $\sqrt{3}a/2$ ) as 6.64 nm. In particular, XRD pattern of  $n = 17$  shows well-ordered mesophase characteristics where  $q$  spacings (meaning inverse  $d$  spacing) are 1.19, 1.72, 2.07, and  $2.34 \text{ nm}^{-1}$  obtained through peak fitting process with Lorentzian profile function. Relative  $q$  spacing is  $\sim 1:\sqrt{2}:\sqrt{3}:2$ . All XRD peaks could be indexed with body-centered cubic phase. Corresponding miller indexes ( $hkl$ ) are (110), (200), (211), and (220), respectively. Cell parameter  $a$  could be estimated with least square method along  $q = [2\pi/a]\sqrt{(h^2 + k^2 + l^2)}$ . This result indicates that pore size increases with increasing alkyl group chain length, concomitant with changing the pore structure from hexagonal cubic to body-centered cubic.  $a$  values for the annealed samples are 3.74, 4.05, 4.39, and 4.91 nm for  $n = 11, 13, 15$ , and  $17$ , respectively. B.C.C structure of  $n = 17$  was changed to hexagonal cubic structure after annealing, and therefore  $d$  spacing value is identical to  $a$  value.

Although peaks shift to the higher angles and decreased intensity after annealing indicates formation of disordered and shrunken mesopores, we can observe the effect of the surfactant alkyl group chain length on the pore size.

High angle X-ray diffraction (XRD) patterns (Fig. 1e and f) of the sample ( $n = 11$ ) confirm the formation of crystalline  $\text{SnHPO}_4$  and  $\text{Sn}_2\text{P}_2\text{O}_7$  phases before and after annealing, respectively (any impurity phases were not detected). These patterns are quite similar to those observed in  $n = 13, 15$ , and  $17$ . This indicates two possibilities; one is the formation of pure mesoporous tin phosphate with pore wall structure consisting of those two crystalline phases, and the other is the formation of a composite consisting of mesoporous and crystalline tin phosphate. The crystalline size of both before and after annealed samples using Scherrer formula was estimated to be  $\sim 50 \text{ nm}$ , which is one order of magnitude larger than the wall thick-

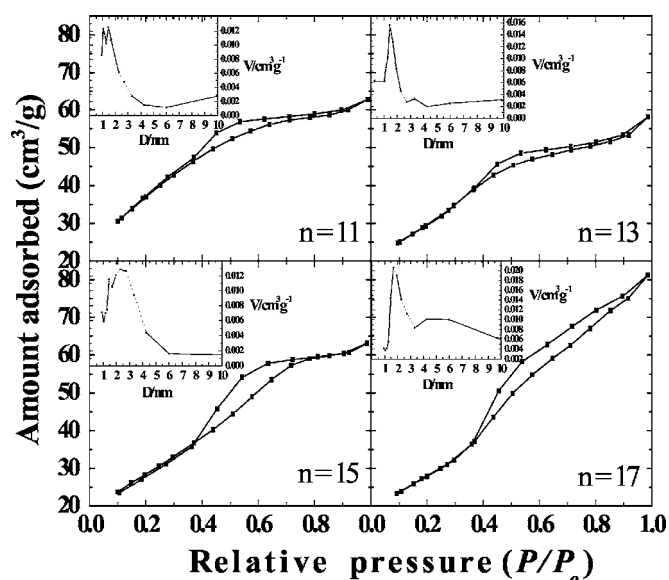


**Figure 2.** Nitrogen adsorption and desorption isotherms of the annealed mesoporous/crystalline tin phosphate prepared using different alkyl chain lengths ( $n = 11, 13, 15$ , and  $17$ ). The corresponding BJH distributions are shown in the inset.

ness of pure mesoporous phase ( $\sim 2 \text{ nm}$ ). These results indicate the formation of a mesoporous tin phosphate mixed with a crystalline phase. Thermogravimetric analysis of the as-synthesized samples under  $\text{N}_2$  flow showed that most of the weight loss occurred at  $400^\circ\text{C}$ , and no weight loss was detected above this temperature, implying that the surfactant could be removed from the mesoporous tin phosphates upon heating at  $400^\circ\text{C}$  for 5 h.

$\text{N}_2$  adsorption-desorption isotherms of the annealed samples in Fig. 2 show the typical curves observed in mesoporous materials. The BET values of  $n = 11, 13, 15$ , and  $17$  are 136, 109, 104, and  $101 \text{ m}^2/\text{g}$ , respectively, and these tend to decrease with increasing alkyl chain length. The mass ratio for mesoporous tin phosphates vs crystalline  $\text{Sn}_2\text{P}_2\text{O}_7$  is  $\sim 1:2$ . This ratio was estimated as follows. First, BET surface area of the crystalline  $\text{Sn}_2\text{P}_2\text{O}_7$  was estimated as  $10 \text{ m}^2/\text{g}$ . Then, BET surface area of the pure mesoporous tin phosphate was estimated from surface area of pore wall/mass of pore wall, and set pore wall size as difference between nearest neighbor distance  $a$  and pore diameter.<sup>17</sup> From these relationships, rough mass ratio of the mesoporous tin phosphate and crystalline  $\text{Sn}_2\text{P}_2\text{O}_7$  can be estimated.

The insets in Fig. 2 show Barrett-Joyner-Halenda (BJH) plots of the annealed samples. The average pore size increased from 1.4, 1.7, 1.9, and 2.2 nm with increasing alkyl chain length, consistent with the SAXS result. More importantly, it should be noted that the trend of pore wall size is coincident with that of pore wall thickness. Pore wall thickness of  $n = 11, 13, 15$ , and  $17$  was estimated to be 2.3, 2.4, 2.5, and 2.7 nm, respectively. Figure 3 exhibits the transmission electron microscopy (TEM) image of the annealed mesoporous tin phosphate prepared using  $n = 17$ . The observed  $d$  spacing value, showing 4.9 nm is similar to the calculated values using SAXS. Pore wall thickness was 2.8 nm.

Figure 4 exhibits voltage profiles of the annealed mesoporous/crystalline composites prepared by surfactant with different alkyl chain lengths, between 0 and 2 V at a rate of 0.2 C ( $1 \text{ C} = 700 \text{ mA/g}$ ). Initial capacities of the samples are similar to each other, showing  $\sim 620$  to  $650 \text{ mAh/g}$ , but capacity retention tends to decrease with increasing pore size and increasing pore wall thickness, as shown in Fig. 5. Accordingly, the sample prepared using  $n = 11$  showed the highest retention value of 82% after 30 cycles. Capacity values of the composite materials are a little higher

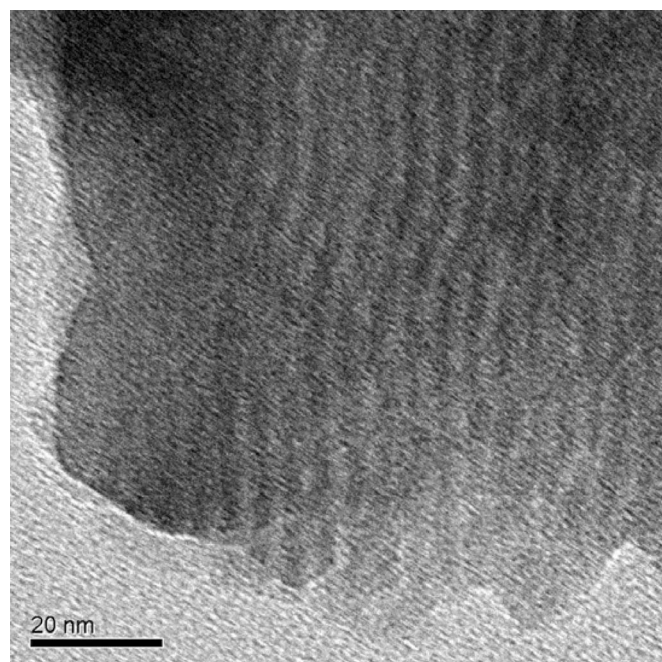


Figure 3. TEM of the annealed mesoporous tin phosphate prepared using  $n = 17$  at  $400^\circ\text{C}$  for 3 h.

than theoretical value ( $\sim 590$  mAh/g). This may be due to larger BET surface area, which facilitates increased lithium reaction sites. Samples prepared using  $n = 13, 15,$  and  $17$  show 67, 63, 59%, respectively (Fig. 6). This trend is expected because shorter chain length induces smaller pore size and pore wall thickness, which in turn, induce smaller expansion/contraction volume of the pore wall from phase transitions between Sn and  $\text{Li}_x\text{Sn}_y$ . Hence, thick pore size with  $n = 17$  showed the worst capacity retention. It was impossible to observe the pore structure of electrodes after 30 cycles due

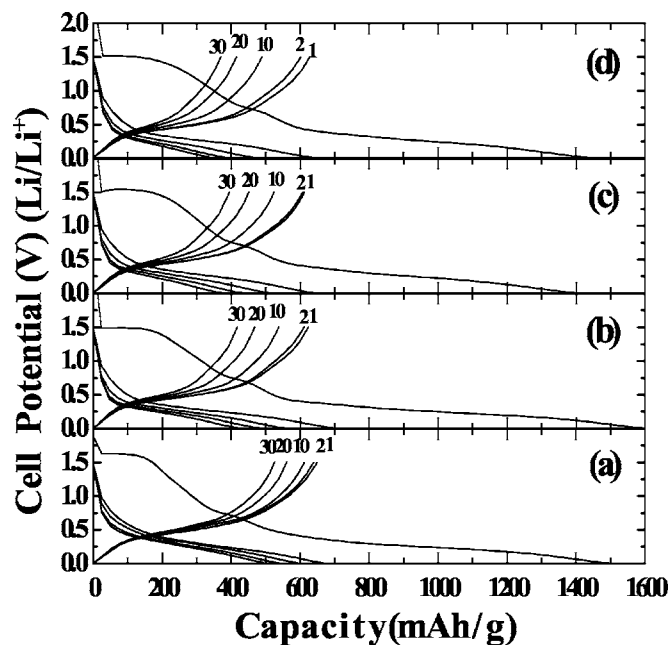


Figure 4. Voltage profiles of the annealed mesoporous/crystalline composites prepared by surfactant with different alkyl chain lengths, between 0 and 1.5 V at a rate of 0.2 C (1 C = 700 mA/g).

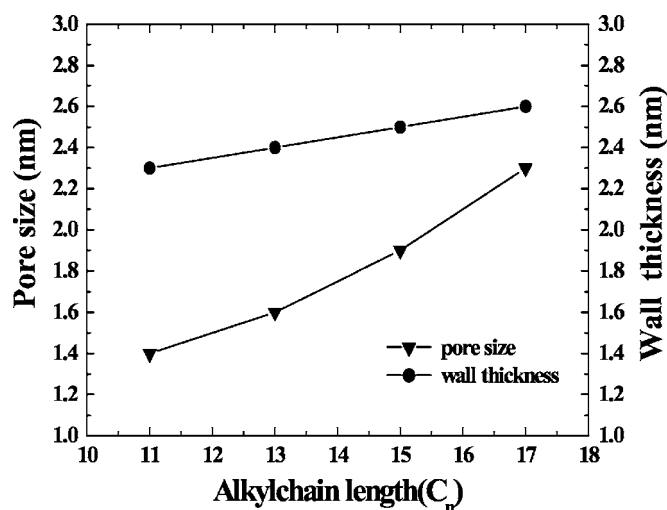


Figure 5. Plots of pore size and pore wall thickness in the mesoporous phase with different alkyl chain lengths.

to severe coverage of the binder and carbon blacks on the mesoporous phases. However, trend of capacity decay clearly shows that smaller pore size/ and thinner pore wall thickness plays a dominant role in deciding capacity retention. One of the critical problems for the mesoporous materials for use in a practical Li-ion cell is relatively large irreversible capacity corresponding to  $\sim 900$  mAh/g during the first cycle. This is believed to be mainly from side reactions with the electrolyte at the interface and may be reduced by coating amorphous carbon on the composite.<sup>18</sup>

### Conclusion

We prepared the mesoporous/crystalline composite containing tin phosphates with different pore sizes and pore wall thickness. Upon decreasing surfactant alkyl chain length, the mesoporous tin phosphate with smaller pore wall size could be obtained. Since smaller pore size and thinner pore wall thickness causes smaller volume change during lithium alloying/dealloying, the composite electrode containing  $n = 11$  showed the highest capacity retention.

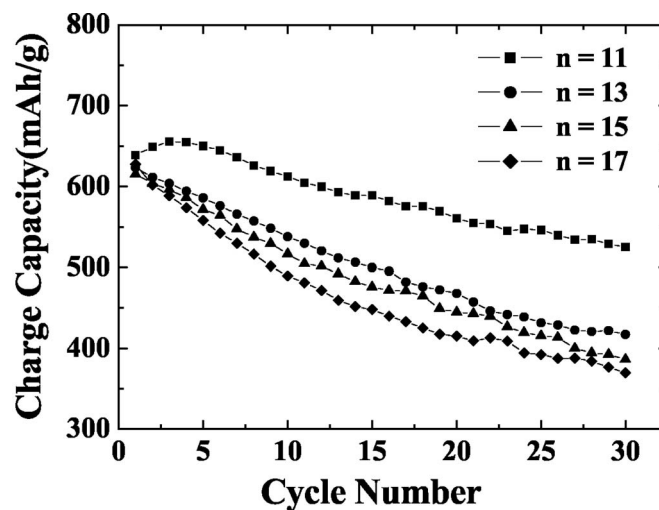


Figure 6. Capacity retention of mesoporous tin phosphate/crystalline  $\text{Sn}_2\text{P}_2\text{O}_7$  composite anode in a coin-type half-cell at a rate of 0.2 C (1 C = 700 mA/g) during 30 cycles.

### Acknowledgments

We are grateful to authorities concerned of Pohang Light Source (PLS) for SAXS measurements. The experiments at PLS were supported in part by Korea MOST and POSTECH. This work was supported by the Basic Research Program (R01-2004-000-10173-0) of KOSEF. This work was also partially supported by University IT Research Center Project.

*Kumoh National Institute of Technology assisted in meeting the publication costs of this article.*

### References

1. C. T. Kresge, M. E. Leonowicz, W. J. Roth, J. C. Vartuli, and J. S. Beck, *Nature (London)*, **359**, 710 (1992).
2. P. Yang, D. Zhao, D. I. Margolese, B. F. Chmelka, and G. D. Stucky, *Nature (London)*, **296**, 152 (1998).
3. P. Behrens, *Angew. Chem., Int. Ed. Engl.*, **35**, 515 (1996).
4. C. Serre, A. Auroux, A. Gervasini, M. Hervieu, and G. Ferey, *Angew. Chem., Int. Ed. Engl.*, **41**, 1594 (2002).
5. S. Cabrera, J. E. Haskouri, C. Guillem, A. Beltran-Porter, D. Beltran-Porte, S. Mendioroz, M. D. Marcos, and P. Amoros, *Chem. Commun. (Cambridge)*, **1999**, 333.
6. S. Cabrera, J. E. Haskouri, J. Alamo, A. Beltran, D. Brltran, S. Mendioroz, M. D. Marcos, and P. Amoros, *Adv. Mater. (Weinheim, Ger.)*, **11**, 5 (1999).
7. T. Katou, D. Lu, J. N. Kondo, and K. Domen, *J. Mater. Chem.*, **12**, 1480 (2002).
8. H. Tanaka and M. Chikazawa, *J. Mater. Chem.*, **9**, 2923 (1999).
9. T. Kimura, Y. Suguhara, and K. Kuroda, *Chem. Commun. (Cambridge)*, **1998**, 559.
10. C. Serre, M. Hervieu, C. Magnier, F. Taulelle, and G. Ferey, *Chem. Mater.*, **14**, 180 (2002).
11. N. K. Mal, S. Ichikawa, and M. Fujiwara, *Chem. Commun. (Cambridge)*, **2002**, 112.
12. F. Chen, Z. Shi, and M. Liu, *Chem. Commun. (Cambridge)*, **2000**, 2095.
13. Z. Peng, Z. Shi, and M. Liu, *Chem. Commun. (Cambridge)*, **2000**, 2125.
14. V. Subramanian, J. C. Jiang, P. H. Smith, and B. Rambabu, *J. Nanosci. Nanotechnol.*, **4**, 125 (2004).
15. E. Kim, D. Son, T. G. Kim, J. Cho, B. Park, K. S. Ryu, and S. H. Chang, *Angew. Chem., Int. Ed. Engl.*, **43**, 5987 (2004).
16. Y. W. Xiao, J. Y. Lee, A. S. Yu, and Z. L. Liu, *J. Electrochem. Soc.*, **146**, 3623 (1999).
17. P. A. Webb and C. Orr, *Analytical Methods in Fine Particle Technology*, Micromeritics Instruments, Norcross, GA (1997).
18. M. Noh, H. Lee, Y. Kwon, J. Cho, Y. Kim, and M. G. Kim, *Chem. Mater.*, **17**, 1926 (2005).